Proposition of a method for measuring and assessing the geometry of an architectural object with a facade covered by a thermal insulation layer

Kinga Wawrzyniak[1], Paulina Modlińska[1], Jaroslaw Wajs[1], Damian Kasza[1, ✉]

[1] Wroclaw University of Science and Technology
✉ Corresponding author: damian.kasza@pwr.edu.pl

Summary

The adverse effects of underground mining often manifest as ground surface deformations, which may lead to damage or even the complete destruction of buildings. Such consequences pose a particularly serious threat to human health, safety, and property. These hazards are mostly monitored and assessed using surveying techniques. This study presents the results of an experimental evaluation of a novel methodology for measuring and estimating the deformation in an architectural structure situated within the mining area of decommissioned coal mines in Upper Silesia (Będzin, southern Poland). The primary research objective was achieved through geodetic measurements employing terrestrial laser scanning (TLS) technology. The proposed measurement procedure comprised two stages: (1) an inventory survey of the building facade, and (2) high-precision scanning of specially designed control points embedded within the thermal insulation layer. Notably, this method effectively compensates for the presence of the thermal insulation, which would otherwise prevent direct measurement of the building's structural surface based on characteristic points.

Keywords

laser scanning technology • mining deformations • monitoring of architectural structures • surveying

1. Introduction

Underground mining activities generate a variety of environmentally adverse effects, collectively referred to as mining-induced damage. Among these phenomena, ground surface deformations are particularly dangerous, as they can cause the dete-

rioration or even irreversible destruction of engineering structures, including buildings and monuments [Florkowska, 2013]. Monitoring such deformations is essential for ensuring public safety, maintaining structural integrity, and preserving cultural heritage.

To address these risks, monitoring systems are implemented to identify endangered areas or structures early, and to assess the magnitude, rate, and spatial extent of deformation over time. In the case of architectural and historic structures – such as churches, historic town halls, or tenement houses – monitoring typically involves a combination of geotechnical methods (e.g., extensometers, inclinometers) [Álvarez-Vigil et al. 2010] and surveying techniques [Bryn et al. 2017].

Classical surveying methods commonly used to monitor the verticality and geometry of building facades include precise levelling and total station measurements. Techniques such as the angular intersection method and the polar method are applied to determine the spatial coordinates of reference points on a structure, providing the basis for evaluating geometric deformations over time [Kuang 1996].

Recent advances in measurement instrumentation and data processing have enabled the development of high-resolution, advanced monitoring techniques, including:
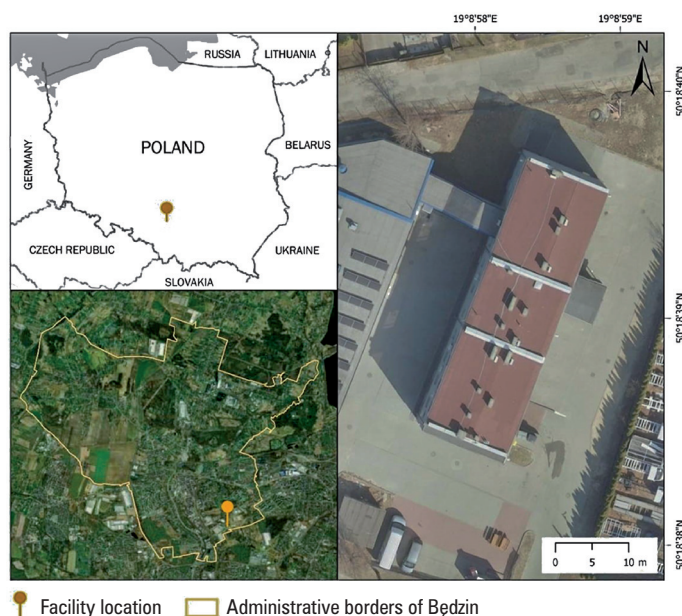
- Terrestrial laser scanning (TLS): used for detailed three-dimensional mapping of structures, TLS enables precise detection of deformations over time [Chen et al. 2022, Mukupa et al. 2017, Li and Wang 2021, Matwij et al. 2021, Mielimąka et al. 2022, Shen et al. 2023],

- Interferometric synthetic aperture radar (InSAR): a remote sensing technique effective for detecting ground movements and deformations over large areas [Cotrufo et al. 2018, Diao et al. 2019, Zhang et al. 2017, Wang et al. 2019, Hu et al. 2024],

- Ground-based radar interferometry (GB-InSAR): applied for continuous real-time monitoring of slope stability and building deformations, providing early-warning capabilities [Semblat et al. 2010, Luzi et al. 2012, Shen et al. 2024],

- Global navigation satellite systems (GNSS): utilized for large-scale deformation monitoring, offering precise measurements of ground displacements [Rodriguez Lloveras et al. 2020, Sokoła-Szewioła et al. 2021, Bo et al. 2023],

- Photogrammetry and unmanned aerial vehicles (UAV): cost-effective methods for monitoring structural deformations [Zheng et al. 2021, Zhou et al. 2020, Jóźków et al. 2021, Tong et al. 2021].

This study presents the results of an experimental investigation aimed at developing and validating a methodology for assessing the deformation of an architectural structure covered with thermal insulation, using terrestrial laser scanning. The selected building is situated in a region that has been significantly affected by underground mining, providing a representative case for evaluating the performance of TLS in comparison to conventional total station measurements.

2. Materials and methods

The selected structure for the tests was a two-story service and technical building located in Będzin, at 73 Zagórska Street (Fig. 1). The building consists of three segments separated by two expansion joints and is connected to an adjacent building at the same address via a covered passage.

The entire structure is clad with a thermal insulation layer, which precludes direct measurement of the geometry of the building's structural body. Notably, the building is situated approximately 250 m northeast of the former Sosnowiec Mine, where coal seams were extracted between 1960 and 1995. This proximity raises concerns that the structure could have been adversely affected by land subsidence or deformation resulting from past mining activity.

Facility location   Administrative borders of Będzin
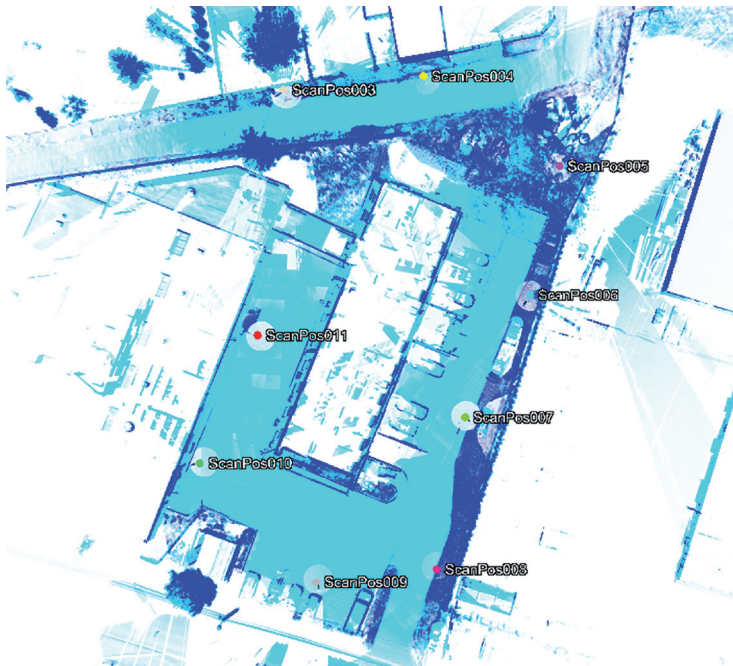
Source: Authors' own study

Fig. 1. Localization of the study object

2.1. Field measurements

Field measurements were conducted using terrestrial laser scanning (TLS) technology, following two distinct procedures. The first procedure, of an inventory nature, was performed with a RIEGL VZ-400i pulse scanner. This instrument integrates two processing systems: the first performs the simultaneous acquisition of scan and image data, along with the execution of system operations; the second provides automatic registration, georeferencing, and data analysis. Together, these systems allow for real-time data regis-

tration. The scanner offers a wide field of view (100° × 360°) and a range of up to 800 m, with a distance measurement accuracy of 5 mm at 100 m. It is also equipped with a GNSS receiver for determining the position of the measuring station. The GNSS system can operate in RTK mode, when connected to a recommended base station, the Internet, or the NTRIP/TCP GNSS correction service. The instrument features a built-in tilt sensor with an accuracy of ±0.008° within a tilt range of ±10°. The first-class laser ensures safe operation, without risk to the human eye. A dedicated mount enables integration of the scanner with a digital camera for panoramic imaging [Riegl 2024].

Data acquisition was carried out in a single measurement session on 2 October 2019. Scans were performed in 'Panorama 50' mode, acquiring approximately 15 million points at a scanning resolution of 0.5°, which corresponds to a theoretical point spacing of about 87 mm at a distance of 10 m from the scanner. The value was calculated according to the resolution settings of the RIEGL VZ-400i used in this study (Fig. 2). Nine measurement stations were positioned to ensure full coverage of the object of interest. Additionally, three control network points were established around the surveyed structure. A local coordinate system was adopted, with the coordinates of the first point set at 100.00 for all components. The positions of the remaining points were determined using total station measurements. This control network was subsequently used during data processing to refine scan alignment.

Source: Authors' own study

Fig. 2. Laser scanner point cloud (RiScan Pro software) showing the study object

The second procedure involved stabilizing and precisely measuring the control network points located directly on the building facade. Each control point consisted of a rod that was inserted through the thermal insulation layer (styrofoam) withal the way to the structural brick wall. A total of sixteen control points were established on the two outermost segments of the building (segments A and C), with four points on each of the eastern and western walls. Dedicated Riegl scanner targets were mounted at the exposed end of each rod, allowing the rod's centre, and thus its exact position, to be determined precisely. The positions of all control points were determined within the local coordinate system. These targets were scanned with the same precision as the reference points during the inventory measurements. Finally, the lengths that each rod protruded beyond the insulation layer were measured using callipers.

2.2. Preliminary data processing

The terrestrial laser scanning (TLS) data acquired in the first stage were subjected to a registration process, i.e., the integration of point clouds from individual measurement stations into a single coherent dataset. Registration was performed in two stages.

In the first stage, automatic registration was carried out using the *Automatic Registration 2* algorithm. This process employed a voxel-based approach, in which the scanned space is divided into finite-size cubes, or three-dimensional pixels [Karbowiak and Kasza 2023]. The voxel size is adjusted according to the characteristics of the scanned object, while the number of voxels defines how many are used in the X, Y, and Z directions during registration. Smaller voxels increase computation time, but may also enhance the accuracy of the results. Given the characteristics of the measurement object, the following parameters were applied:

1. Registration mode: Outdoor Urban (optimized for urban areas),
2. Voxel size: 0.25 m.

The second stage involved refining the alignment of all point coordinates using the *Multi Station Adjustment 2* algorithm. This step incorporated all available measurements and control points, enabling the spatial dataset to be referenced against an external coordinate system—in this case, the local datum. The following conditions were adopted to ensure accurate processing:

1. Control points were recorded at 11 scan stations,
2. The distance between scan stations did not exceed 10 m (urban environment),
3. A minimum overlap of 30% was maintained between adjacent scans.

Upon completion of the registration process, the resulting dataset comprised over 587 million points.

3. Results

After completing the preliminary processing of the point cloud representing the studied object, seven cross-sectional lines were extracted from the western elevation of the

building (Fig. 3A) and six from the eastern elevation (Fig. 3B). Two vertical cross-sections were created for each building segment (labeled A, B, and C; with segment A located on the north side) on both the east and west sides, except for the third outer-most cross-section on the west side, where three cross-sections were generated.

Source: Authors' own study

Fig. 3. East elevation (A) and west elevation (B) – point cloud with designed profiles marked by red lines

In most cases, the cross-sections were positioned to pass through stabilized control points, enabling a comparison of tilt values obtained from the two measurement procedures. This was not possible for the middle segment (segment B), where no control points had been installed.

The coordinates of the extreme points on each cross-section were extracted in the local coordinate system (Table 1). The tilt of each line was then calculated using the coordinates of the cross-sectional line with the lowest elevation ordinate as a reference. This reference point was selected because it is closest to the ground level in each profile. This minimizes the influence of potential vertical offsets between scans and ensures that tilt values reflect true deviations from verticality rather than differences in elevation origin. For subsequent analysis, an average survey line length of 5.8 m was adopted, corresponding to the mean length of all cross-sectional lines.

The proposed measurement procedure was designed to determine the tilt of the building structure. For this purpose, 300 mm measuring rods were inserted through the insulation layer at four measurement profiles in the analysed locations. After recording the length of the protruding portion of each rod with a calliper, the structural tilt was calculated according to equation (1):

$$True\_tilt = A - B + Tilt\_TLS \tag{1}$$

**Table 1.** Coordinates of the extreme points of the designated cross-sectional lines

Cross-sectional line number	West wall			East wall		
	X [m]	Y [m]	Z [m]	X [m]	Y [m]	Z [m]
1 – bottom	51.610	120.357	101.926	52.955	108.902	101.990
1 – top	51.511	120.349	107.866	53.062	108.895	107.751
2 – bottom	57.122	120.213	101.904	60.821	108.623	102.005
2 – top	57.056	120.221	107.865	60.831	108.618	107.661
3 – bottom	63.866	120.050	101.856	–	–	–
3 – top	63.833	120.046	107.827	–	–	–
4 – bottom	64.874	119.990	101.941	68.266	108.374	102.030
4 – top	65.009	119.984	107.626	68.420	108.381	107.609
5 – bottom	73.896	119.824	101.774	73.392	108.270	101.800
5 – top	73.899	119.831	107.771	73.412	108.267	107.494
6 – bottom	75.626	119.774	101.746	75.288	108.214	101.766
6 – top	75.581	119.770	107.641	75.311	108.206	107.484
7 – bottom	87.310	119.587	101.714	87.230	108.048	101.689
7 – top	87.270	119.595	107.508	87.356	108.047	107.271

Table 2. Tilt values of the designated cross-sectional lines

Cross-sectional line number	Building construction with thermal insulation layer		True building construction	
	West wall	East wall	West wall	East wall
	tilt [mm/m]			
1	−1.4	−1.2	−8.3	−12.6
2	1.4	−0.9	0.7	−17.0
3	−0.7	–	–	–
4	1.0	1.2	–	–
5	1.2	−0.5	–	–
6	−0.7	−1.4	−0.9	−12.7
7	1.4	−0.2	−1.0	−11.0

The calculation scheme for determining the building's structural tilt is presented in Fig. 4. For each profile (cf. Fig. 3), tilt values were obtained using the laser scanning method. These values, denoted as *Tilt_TLS* for profiles #1 through #7, did not exceed 1 cm.

Variations in the depth of the penetration of the rod into the insulation layer indicate the inclination of the building. By incorporating the measured rod depressions into the calculations, the relative building tilt was determined for each profile in millimeters per meter (right column in Table 2).
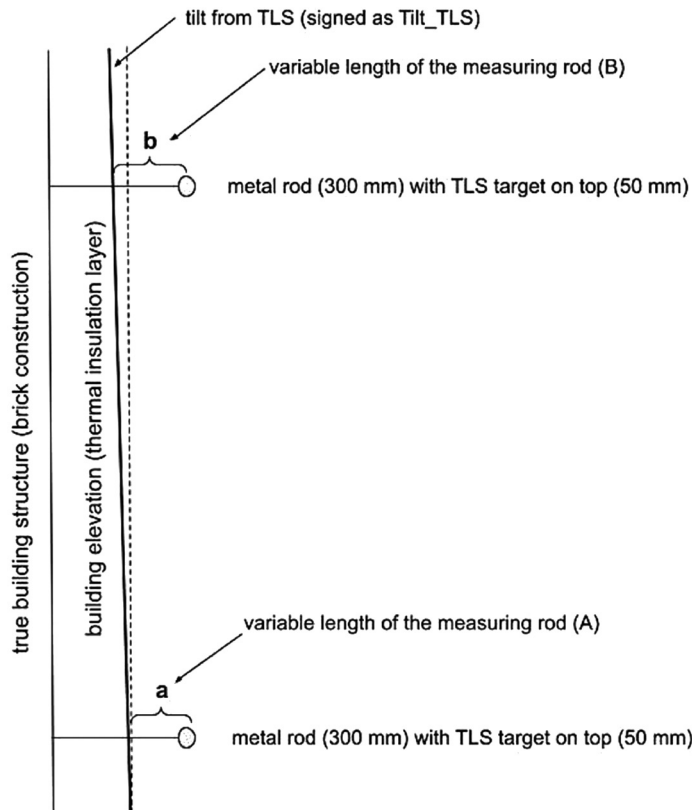
Source: Authors' own study

Fig. 4. Graphical representation of the method of calculating the relative tilt of a building structure using a metal rod with a 50 mm reference target in a selected vertical cross-section

4. Discussion

LiDAR data provide the capability to monitor the elevation of a structure and detect potential deformations. For instance, Gawronek and Makuch [2019] compared TLS measurements during static loading of a bridge with classical methods (levelling, total

station, etc.). They found that differences between TLS and highly precise levelling were within ±2.8 mm at a 95% confidence level. While the accuracy of TLS for individual points was estimated at ±2–20 mm, modelling entire surfaces allowed deformations to be captured more precisely through global point cloud analysis. This confirms that TLS can reliably complement classical methods, particularly when monitoring entire structural surfaces. The classical approach uses LiDAR measurements derived from movements of the building, which allows for relative displacement analysis (Table 2). However, it does not enable direct assessment of the building's structural elements. Examination of Figure 5a indicates that the overall body of the building has a tilt of no more than 1 mm/m. Similar results can be obtained from LiDAR measurements taken at any location on the facade, including areas covered with thermal insulation. This is likely due to the insulation being installed correctly.

In contrast, Figure 5b – based on the developed methodology – reveals that the tilt of individual building segments reaches values of up to 17 mm/m. The direction of the tilt vector, calculated from the control point data, is consistent for segments A and C. Although no steel rods were installed in segment B for this study, it cannot be ruled out that a similar process is occurring in the central portion of the structure. From a structural perspective, it is noteworthy that segment A exhibits uneven leaning between the paired profiles on the west and east sides, which may indicate localized structural irregularities.
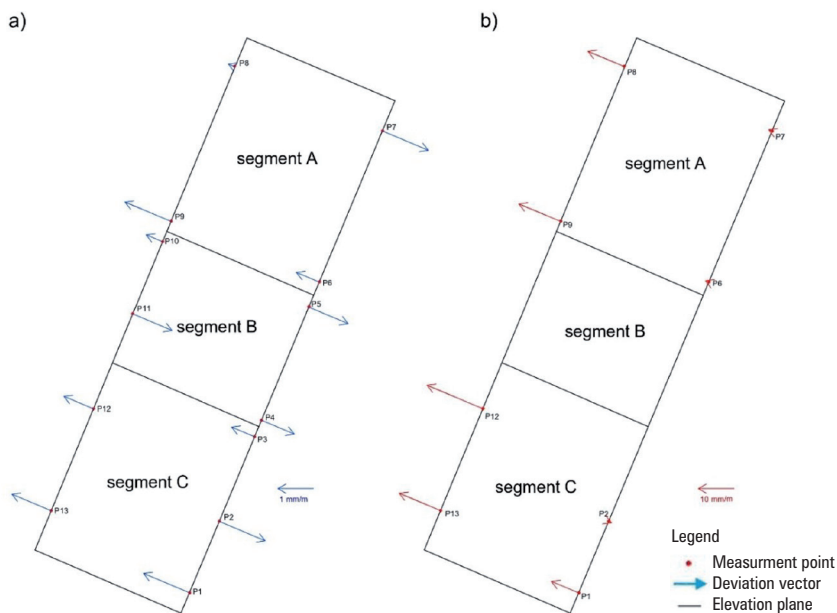
Source: based on the Authors' procedure with steel rods

Fig. 5. Visualization of the calculated tilt vectors for the designated cross-sectional lines of the test object: (a) including the thermal insulation layer (based on direct TLS measurements), (b) excluding the thermal insulation layer

5. Conclusions

The results obtained from direct measurements of the building using classical surveying techniques do not allow us to determine whether the structure has experienced significant tilting, nor can they indicate when or why such tilting occurred. The measurements conducted represent only an initial (pilot) series. To achieve a comprehensive assessment, periodic measurements would be required (e.g., on an annual basis), taking into account the current mining and geological conditions during interpretation.

It is important to note that the proposed measurement method – based on precise monitoring of control points in the form of steel rods – can provide reliable results with a high level of confidence, as measurement accuracy is determined by the employed technique. During the conducted experiment, particular attention was paid to ensuring perpendicular installation of the rods in order to reduce the possibility of measurement errors. In practical conditions, however, it is not possible to completely eliminate certain deviations, which may result in minor systematic errors in the localization of control points, especially in the long-term assessment of deformation. This can be considered a potential limitation of the method. It should be taken into account in further studies, for example in an analysis of the influence of variable rod inclination angles on measurement accuracy. The optimal solution for this type of analysis would involve permanently mounted reference rods, although this is an invasive approach. The method proposed here remains primarily based on non-contact LiDAR scanning, but it requires the temporary installation of a control-measurement network. The length of the measuring rods (30 cm in this study) was selected based on the insulation documentation or, alternatively, determined through a test hole. This methodology enables precise representation of the building structure in the form of cross-sections.

The authors recommend periodic monitoring of the structure using steel rods. If future monitoring is performed using raw LiDAR data alone (e.g., via the ICP method), an accurate interpretation of additional tilting is feasible, provided that the thermal insulation layer is properly installed – i.e., it adheres firmly to the masonry and does not form a detached surface. In such case, the rod-based approach offers a more universal solution, guaranteeing absolute measurements of structural tilt.

References

Álvarez-Vigil A.E., González-Nicieza C., López Gayarre F., lvarez-Fernández M.I. 2010. Forensic analysis of the evolution of damages to buildings constructed in a mining area (Part II). Engineering Failure Analysis, 17(4), 938–960. https://doi.org/10.1016/j.engfailanal.2009.11.005

Bo H., Li Y., Tian X. 2023. Estimation of ground subsidence deformation induced by underground coal mining with GNSS IR. Remote Sens.,15(1), 96.

Bryn M.J., Afonin D.A., Bogomolova N.N. 2017. Geodetic Monitoring of Deformation of Building Surrounding an Underground Construction. Procedia Engineering, 189, 386–392. https://doi.org/10.1016/j.proeng.2017.05.061

Chen Z., Zhang W., Huang R., Dong Z., Chen C., Jiang L., Wang H. 2022. 3D model-based terrestrial laser scanning (TLS) observation network planning for large-scale building facades. Automation in Construction, 144, 104594. https://doi.org/10.1016/j.autcon.2022.104594

Cotrufo S., Sandu C., Giulio Tonolo F., Boccardo P. 2018. Building damage assessment scale tailored to remote sensing vertical imagery. European Journal of Remote Sensing, 51(1), 991–1005. https://doi.org/10.1080/22797254.2018.1527662

Diao X., Wu K., Chen R., Yang J. 2019. Identifying the Cause of Abnormal Building Damage in Mining Subsidence Areas Using InSAR Technology. IEEE Access, 7, 172296–172304. https://doi.org/10.1109/ACCESS.2019.2956094

Florkowska L. 2013. Example building damage caused by mining exploitation in disturbed rock mass. Studia Geotechnica et Mechanica, 35(2), 19–37. https://doi.org/10.2478/sgem-2013-0021

Gawronek P., Makuch M. 2019. TLS Measurement during Static Load Testing of a Railway Bridge. ISPRS International Journal of Geo-Information, 8(1), 44. https://doi.org/10.3390/ijgi8010044

Hu L., Tang X., Tomás R., Li T., Zhang X. 2024. Monitoring surface deformation dynamics in the mining subsidence area using LT 1 InSAR interferometry: A case study of Datong, China. Int. J. Appl. Earth Obs. Geoinf., 131, 103936.

Jóźków G., Walicka A., Borkowski A. 2021. Monitoring terrain deformations caused by underground mining using UAV data. Int. Arch. Photogramm. Remote Sens. Spatial Inf. Sci., XLIII-B2, 737–744.

Karbowiak K., Kasza D. 2023. Application of Terrestrial Laser Scanning in Inventories of Architectural Objects and Building Structures – Illustrated by St. Lazarus' Church in Wrocław (Poland). IOP Conference Series: Earth and Environmental Science, 1189(1), 012029. https://doi.org/10.1088/1755-1315/1189/1/012029

Kuang S. 1996. Geodetic network analysis and optimal design: concepts and applications.

Li J., Wang L. 2021. Mining subsidence monitoring model based on BPM EKTF and TLS and its application in building mining damage assessment. Environ. Earth Sci., 80, 396.

Luzi G., Crosetto M., Fernández E. 2012. Ground-Based Radar Interferometry: A bibliographic review. Remote Sens., 4(9), 2750–2780.

Matwij W., Gruszczyński W., Puniach E., Ćwiąkała P. 2021. Determination of underground mining induced displacement field using multi temporal TLS point cloud registration. Measurement, 180, 109482.

Mielimąka R., Sikora P., Mazur P. 2022. The use of TLS technology in the inventory of damage to building objects resulting from the impact of underground mining exploitation. XXVII FIG Congress: Volunteering for the Future ‑ Geospatial Excellence for a Better Living (FIG Congress 2022).

Mukupa W., Roberts G.W., Hancock C.M., Al Manasir K. 2017. A review of the use of terrestrial laser scanning application for change detection and deformation monitoring of structures. Surv. Rev., 49, 99–116.

Riegl VZ-400i. 2024. Series datasheet. https://www.Laser-3d.Pl/Riegl-Tls/Riegl-vz-400i [accessed: 10.06.2024].

Rodriguez-Lloveras X., Puig-Polo C., Lantada N., Gili J.A., Marturià J. 2020. Two decades of GPS/GNSS and DInSAR monitoring of Cardona salt mines (NE Spain) – natural and mining-induced mechanisms and processes. Proc. IAHS, 382, 167–172.

Semblat J.F., Kham M., Parmentier J.F., Luong M.P. 2010. Local amplification of deep mining induced vibrations – Part 2: Simulation of the ground motion in a coal basin. arXiv preprint., arXiv:1005.3249.

Shen N., Wang B., Ma H., Zhao X., Zhou Y., Zhang Z., Xu J. 2023. A review of terrestrial laser scanning (TLS)-based technologies for deformation monitoring in engineering. Measurement, 223, 113684. https://doi.org/10.1016/j.measurement.2023.113684

Shen Y., Zhang Y., Li Y., Li Z., Li X. 2024. Integration of ground-based radar and satellite InSAR data for the analysis of an unexpected slope failure in an open-pit mine. Environ. Earth Sci., 83(112), 1–17.

Sokoła-Szewioła V. et al. 2021. Validation of the accuracy of geodetic automated measurement system based on GNSS platform for continuous monitoring of surface movements in post-mining areas. Rep. Geod. Geoinf., 112(1), 47–57.

Tong X., Zhang Y., Zhao J., Wang Q. 2021. Novel method for monitoring mining subsidence featuring co-registration of UAV LiDAR data and photogrammetry. Appl. Sci., 12(18), 9374.

Wang C., Zhang Z., Zhang H., Wu Q., Zhang B., Tang Y. 2019. Application of InSAR time-series analysis for the assessment of mining induced structural damage in Panji Mine, China. Nat Hazards.

Zhang A., Lu J., Kim J.W. 2017. Detecting mining induced ground deformation and associated hazards using spaceborne InSAR techniques. Geomat. Nat. Hazards Risk.

Zheng Z., Zhong Y., Wang J., Ma A., Zhang L. 2021. Building damage assessment for rapid disaster response with a deep object-based semantic change detection framework: From natural disasters to man-made disasters. Remote Sensing of Environment, 265, 112636. https://doi.org/10.1016/j.rse.2021.112636

Zhou D., Qi L., Zhang D., Zhou B., Guo L. 2020. Unmanned Aerial Vehicle (UAV) photogrammetry technology for dynamic mining subsidence monitoring and parameter inversion: A case study in China. IEEE Access, 8, 16372–16386.